

## Old Dominion University ODU Digital Commons

---

Bioelectrics Publications

Frank Reidy Research Center for Bioelectrics

---


2017

# Biochemical and Histological Differences Between Costal and Articular Cartilages

Michael W. Stacey

Old Dominion University, [mstacey@odu.edu](mailto:mstacey@odu.edu)

Follow this and additional works at: [https://digitalcommons.odu.edu/bioelectrics\\_pubs](https://digitalcommons.odu.edu/bioelectrics_pubs)

 Part of the [Biochemistry Commons](#), [Biomedical Engineering and Bioengineering Commons](#), and the [Molecular Biology Commons](#)

---

### Repository Citation

Stacey, Michael W., "Biochemical and Histological Differences Between Costal and Articular Cartilages" (2017). *Bioelectrics Publications*. 215.

[https://digitalcommons.odu.edu/bioelectrics\\_pubs/215](https://digitalcommons.odu.edu/bioelectrics_pubs/215)

### Original Publication Citation

Stacey M.W. (2017) Biochemical and histological differences between costal and articular cartilages. In A. K. Saxena A. (Ed.), Chest Wall Deformities (pp 81-99): Springer Verlag.

This Book Chapter is brought to you for free and open access by the Frank Reidy Research Center for Bioelectrics at ODU Digital Commons. It has been accepted for inclusion in Bioelectrics Publications by an authorized administrator of ODU Digital Commons. For more information, please contact [digitalcommons@odu.edu](mailto:digitalcommons@odu.edu).

## Metadata of the chapter that will be visualized online

|                               |   |
|-------------------------------|---|
| Chapter Title                 | Biochemical and Histological Differences between Costal and Articular Cartilages  |
| Copyright Year                | 2017  |
| Copyright Holder              | Springer-Verlag Berlin Heidelberg   |
| Corresponding Author          | Family Name <b>Stacey</b>   |
|                               | Particle  |
|                               | Given Name <b>Michael W.</b>  |
|                               | Suffix  |
|                               | Division Frank Reidy Research Center for Bioelectrics   |
|                               | Organization/University Old Dominion University   |
|                               | Address 4211 Monarch Way, Suite 300, Norfolk, VA 23508, USA   |
|                               | Email mstacey@odu.edu   |
| Abstract                      | Biologically, costal cartilage is an understudied tissue type and much is yet to be learned regarding underlying mechanisms related to form and function, and how these relate to disease states, specifically chest wall deformity. Chest wall deformities have a component of inheritance, implying underlying genetic causes; however the complexity of inheritance suggests multiple genetic components. At our Centre investigations were performed on gene expression of key select genes from costal cartilage removed at surgery of patients with chest wall deformity to show high expression of decorin, a key player in collagen fiber formation and growth. Also, the degree of tissue differentiation was investigated that was different to that of articular cartilage as measured by gene ratio. Ultrastructural aspects of costal cartilage were determined by scanning and atomic force microscopy to show the presence of ‘nanostraws’ and preliminary data of nanostraw strength by measuring Young’s modulus of individual nanostraws. Protein deposition of collagen type II, decorin, and biglycan suggest orchestration of fiber formation in the interterritorial matrix. Although no specific biological markers related to chest wall deformity have currently been identified, work from our Centre has identified potential areas of interest. |
| Keywords (separated by “ - ”) | Costal cartilage - Chondrocytes - Collagen - Aggrecan - Decorin - Biglycan - SLRP - Glycosylation - Scanning electron microscopy - Atomic force microscopy - Gene expression  |

# Biochemical and Histological Differences between Costal and Articular Cartilages

7

Michael W. Stacey

## Abbreviations

|        |   |
|--------|---|
| AFM    | Atomic Force Microscope                         |
| cDNA   | Complimentary Deoxyribonucleic Acid             |
| DNA    | Deoxyribonucleic Acid                           |
| ECM    | Extra Cellular matrix                           |
| FCD    | Fixed Charge Density                            |
| GAG    | Glycosaminoglycan                               |
| MMP    | Matrix Metalloproteinase                        |
| PBS    | Phosphate Buffered Saline                       |
| PC     | Pectus Carinatum                                |
| PCR    | Polymerase Chain Reaction                       |
| RNA    | Ribonucleic Acid                                |
| RT-PCR | Reverse Transcriptase Polymerase Chain Reaction |
| SEM    | Scanning Electron Microscope                    |
| SLRP   | Small Leucine Rich Proteoglycan                 |
| SNP    | Single Nucleotide Polymorphism                  |
| VNTR   | Variable Number of Tandem Repeats               |

M.W. Stacey, PhD  
Frank Reidy Research Center for Bioelectrics,  
Old Dominion University, 4211 Monarch Way,  
Suite 300, Norfolk, VA 23508, USA  
e-mail: [mstacey@odu.edu](mailto:mstacey@odu.edu)

## Introduction

Costal cartilages, a type of hyaline cartilage, are bar like structures connecting the ribs to the sternum and allows for rib cage flexibility. Unlike articular cartilage of the joints, which is only a few mm thick, costal cartilage can approach approximately 1 cm in diameter. Like other cartilage types, the body of the tissue does not have nerve or blood supplies. Costal cartilage does have a surrounding perichondrium that is vascular and provides nutrients. Nutrients diffuse into the cartilage, but it is estimated that diffusion coefficients are in the order of 200 mm, a fraction of the diameter of costal cartilage. This results in a dilemma regarding costal cartilage structure and function. Centrally located cells are deprived of oxygen and cell metabolism creates an acidic environment. Indeed, chondrocyte gene expression is up regulated in these conditions, and needs to be accounted for in future experiments; however, cells still require some minimal nutrient and gas exchange to function. Our group examined costal cartilage immunohistochemically and by scanning electron microscopy to determine the structure and protein content of costal cartilage, and genetically by examination of gene expression of key cartilage related genes.

25

26 [AUT](#)

27

28

29

30

31

32

33

34

35

36

37

38

39

40

41

42

43

44

45

46

47

48

49

50

51

52

52

## 53 Cellular Distribution

54 Histologically, the proteins of cartilage are produced by chondrocytes that are sparsely distributed throughout the secreted extra cellular matrix (ECM), occupying only approximately 2% of cartilage. Few studies have been undertaken on chondrocyte distribution within cartilage, yet cell density and arrangements are considered to be critical to function. Cellular clusters [1], pairs [2], and rows [3], have been reported. A more extensive study [4] in the superficial zone of articular cartilage identified complex patterns that appear to be location specific. For example, chondrocytes of the articular surface of ankle joints were as pairs, whereas strings of chondrocytes were found in half of the superficial chondrocytes of the femoral condyles of the knee joint, and circular clusters were found in the patella-femoral groove of the femur [4]. It has been suggested that chondrocyte groups form after cell division with incomplete separation within the cellular microenvironment allowing direct communication between cells [5]. In cross sections of costal cartilage removed from a patient with pectus carinatum we observed 98% of cells were single or paired towards the periphery whereas 8% appeared as clusters of 3–4+ cells in central regions, consistent with the notion that younger cells that have undergone one or no divisions are peripheral, with older cells having undergone more divisions being embedded more centrally. In a control sample, ~13% of cells were in clusters of 3–4+ in central regions. Although the control sample showed cell clusters nearly twice that of a PC sample, verification of rib number and site was not possible, and thus in this instance site specific variation cannot be confirmed. No strings were observed in PC or control sample. A spatial relationship between collagen fiber alignment and cellular organization has been suggested [3], with chondrocytes running parallel to adjacent fibers. When we examined longitudinal sections of costal cartilage, we also note the presence of lacunae between the large fibrous structures [6]. The predominance of single and doublets in costal cartilage suggests cells undergo relatively few divisions. The absence of extensive strings and

clusters is likely due to the different biomechanical forces experienced by costal cartilage compared to articular cartilage of joints.

The forces experienced by costal cartilages are very different to those of load bearing cartilage and a comprehensive investigation of the cellular distribution along the length of individual costal cartilages may reveal important insights into apparent weaknesses observed in patients with chest wall deformities.

## Costal Cartilage Structure

### Collagen Type IIA1 (COL2A1) Presence in Costal Cartilage

Recent work [7] described a decrease in the biomechanical stability of costal cartilage in pectus excavatum patients and suggested a disorderly arrangement and distribution of collagen fibers. Other authors have suggested that atypical collagen fibers may be implicated in chest wall deformities [8, 9]. The arrangement of collagen fibers in costal cartilage has not been described in detail; however, highly ordered fiber formation was described in the surrounding perichondrium [10]. A lack of understanding of molecular and ultrastructural properties hampers understanding events leading to these disorders.

Collagen type II is a major constituent of hyaline cartilage, consisting of ~70% of cartilage dry weight. It is a fibrous protein that is cross-linked to other fibers and adds structure and strength. Mutations in collagen genes have been described in many skeletal dysplasias, but no abnormalities have been described in patients with chest wall deformities. The presence of COL2A1 in costal cartilage is shown in Fig. 7.1. Staining appears to be intense surrounding cellular lacunae, with a more uniform staining pattern within the matrix. This staining is consistent with COL2A1 staining in hyaline cartilage. Negative controls showed no staining (data not shown).

### Aggrecan Presence in Costal Cartilage

Aggrecan, a large proteoglycan present at 3–10% cartilage dry weight, serves as an attachment for chondroitin and keratin sulphates,

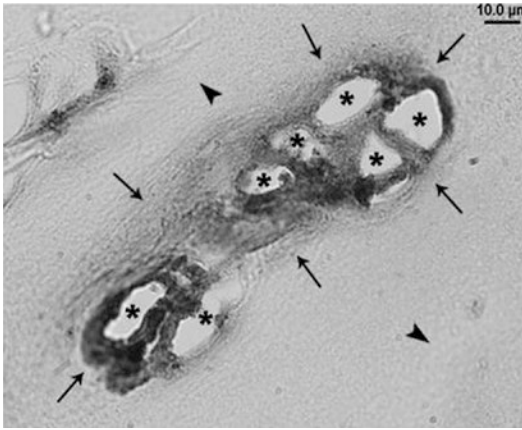


**Fig. 7.1** Immunohistochemistry using a COL2A1 specific human monoclonal antibody showing intense COL2A1 staining (*arrows*) around cellular lacunae (\*), with a lighter, more uniform COL2A1 stain over the matrix (*arrow heads*) [44]

negatively charged environment draws in water and cations, e.g., Na<sup>+</sup> that was confirmed by Electron Probe Micro Analysis in a section of costal cartilage (Fig. 7.3).

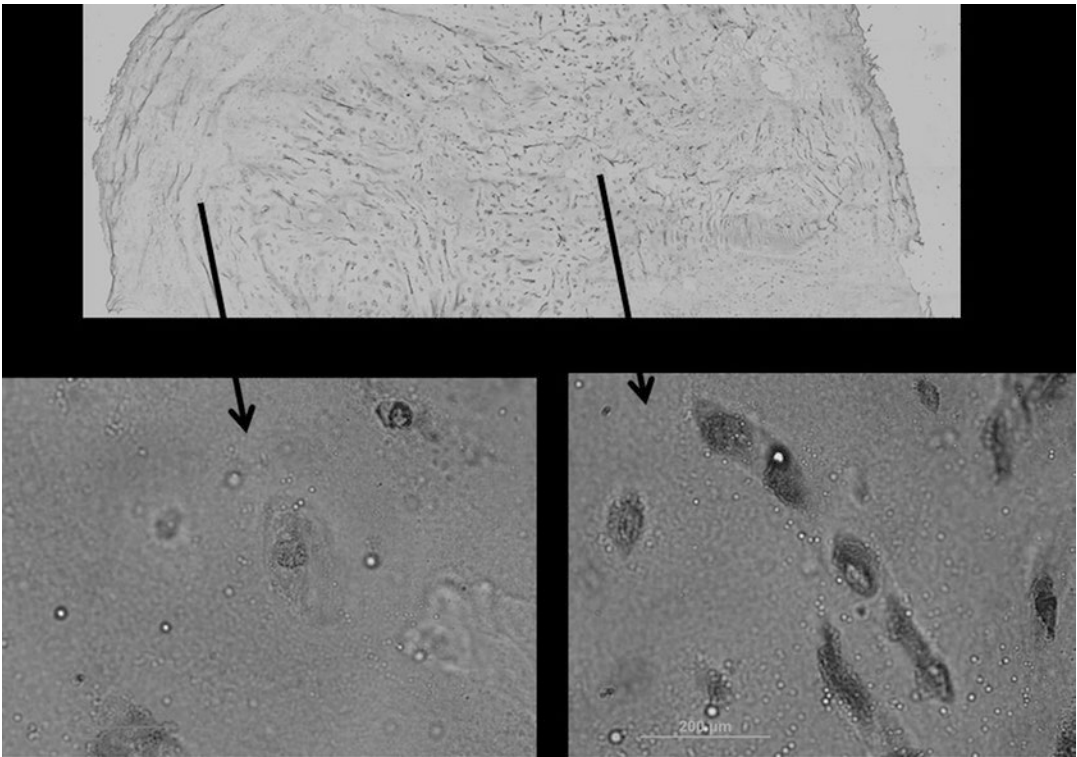
Although collagens and aggrecan are major protein constituents of cartilage, major differences between articular cartilage and costal cartilage in form and function are very apparent and thus major differences in protein content and deposition are expected. The presence and driving force of aggrecan and associated negatively charged proteins are common to both; however the arrangement of collagen fibers in response to their unique sites primarily reflect function. This draws the question as to how fibers are arranged in costal cartilage, and what proteins may play a role in the process of fibrillogenesis.

highly negatively charged proteins that are responsible for the fixed charge density of cartilage. This fixed charge density (FCD) is the source of all electrochemical events in cartilage [11] and is responsible for cation movement into the tissue along with water to produce osmotic swelling that gives cartilage its unique physical properties. Abnormalities in aggrecan can result in weakened cartilage, as exemplified in osteoarthritis where breakdown of aggrecan, reduced FCD, and associated reduction in osmotic pressure, result in weakened cartilage susceptible to wear and tear.

Hypoxia or low pH has been shown to act as a trigger for aggrecan production through induction of hypoxia inducible factor 1- $\alpha$  and *SOX9*, as well as inhibit *COL1A1* expression [12, 13]. Similarities with inter vertebral discs are noteworthy. Cells embedded within the centrally located nucleus pulposus experience hypoxia and express aggrecan under the regulation of the hypoxia induced P13K/AKT signaling pathways via modulation of *SOX9* [14]. It appears that as cells become centrally located they, due to lack of blood supply, experience hypoxia and lower pH. Consistent with this hypothesis, we observed aggrecan deposition by chondrocytes in centrally located regions of costal cartilage compared to those cells at the periphery (Fig. 7.2). The induced

### Small Leucine Rich Proteoglycans (SLRPs)

Small leucine rich proteoglycans (SLRPs) are extra cellular matrix molecules that bind strongly to collagen and other matrix molecules. They are associated with collagen fibril formation and therefore important in the proper formation of ECMs. The co-operation, sequential, timely, orchestrated action of SLRPs that shape architecture and mechanical properties of the collagen matrix and overall importance in disease is reviewed by Ameye and Young [15]. Indeed, SLRP knockout mice exhibit disorganized collagen fibers and loss of connective tissue function [16, 17]. Fragmentation of SLRPs is associated with degeneration of matrix in meniscus, knee and hip cartilage [18]. The name arises from their relative small size of approximately 40 kDa compared to ~200 kDa for the large aggregating proteins aggrecan and versican, the presence of numerous adjacent leucine rich repeats and one or very few glycosaminoglycan (GAG) side chains. SLRPs are generally expressed in a very tissue specific manner. Mechanistically, it is accepted that horseshoe shaped SLRPs interact with individual collagen fibrils by their concave surfaces, and the space inside the horseshoe accommodates a single tri-



AU6

AU2

**Fig. 7.2** Localization of aggrecan by immunohistochemistry in transverse cross-sections of costal cartilage. (a) Distribution of aggrecan in whole control section. (b) Distribution of aggrecan in whole PC3 section. (c–e) Distribution of aggrecan in control at 10× magnification from (c) periphery, (d) midzone, and (e) interior regions. (f–h) Distribution of aggrecan in control at 100× magnification from (f) periphery, (g) midzone, and (h) interior regions. Scale bars, 100 μm. Notice the localization of aggrecan becomes more intense around each lacuna in the interior compared to the periphery

218 ple helix of collagen [15]. Mutations in SLRPs  
 219 may be important as predisposing genetic factors  
 220 for diseases of the ECM.

221 Reports of decreased biomechanical stability  
 222 of costal cartilage in pectus excavatum and sug-  
 223 gested disorderly arrangement, distribution, and  
 224 atypical collagen fibers in chest wall deformities  
 225 [7–9], led us to examine the size and distribution  
 226 of two SLRPs expressed in cartilage, decorin and  
 227 biglycan [19]. Both regulate ECM growth and  
 228 fibrillogenesis. Interestingly, both sequester  
 229 TGFβ, controlling availability of this growth fac-  
 230 tor and thus growth of cartilage. The important  
 231 roles of decorin and biglycan in fibrillogenesis  
 232 and sequestration of TGFβ makes them interest-  
 233 ing molecules to investigate in disorders related  
 234 to abnormal cartilage growth and strength. There  
 235 may be a mechanistic role for these two SLRPs in

chest wall deformity. Decorin and biglycan are 236  
 prominent class I members of the SLRP family 237  
 and are homologous (57% identity at the amino 238  
 acid level) but with divergent patterns of expres- 239  
 sion. Despite their similarities, biglycan and 240  
 decorin have distinct functions which may par- 241  
 tially result from differences in GAG chains; big- 242  
 lycan has two chondroitin sulphate chains and 243  
 decorin has one, respectively (Fig. 7.4a, b). 244

245 Biglycan deficiency has been shown to cause 246  
 spontaneous aortic dissection and rupture in mice 247  
 [20], a characteristic of Marfan syndrome, a syn- 248  
 drome known to exhibit chest wall deformities. 249  
 Decorin function is consistent with functions 250  
 related to fibrillogenesis [17, 21]. Null mutations 251  
 lead to abnormal collagen architecture in mice 252  
 suggesting a mechanistic role for these proteins 253  
 in skeletal disorders.

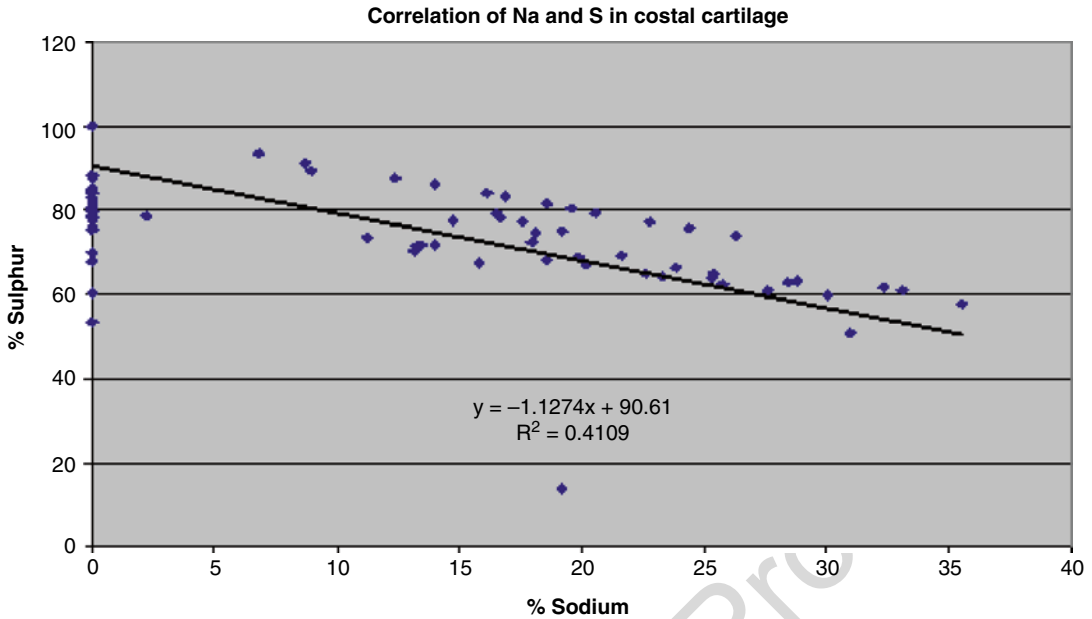


**Fig. 7.3** Electron probe microanalysis of 100 equally spaced points over a transverse section of costal cartilage. Sodium is present only in the central 48 points (*boxed*), and not at the peripheral points, which contain Sulphur only (*circled*) showing that positively charged ions were drawn to central regions to achieve electroneutrality [6]

254        Decorin and biglycan have different isoforms,  
 255 the pro and mature forms that show differential  
 256 expression [22–24]. Proforms have a 14 amino  
 257 acid N-terminal pro-peptide that is cleaved in the  
 258 mature forms. The abundance of pro-forms of  
 259 both SLRPs is tissue and age dependent, with the  
 260 mature form being expressed more highly in  
 261 juvenile tissue, and the pro form in adult [25, 26].  
 262 Structurally, costal cartilage has been shown to  
 263 consist of straw-like structures running parallel  
 264 to the length of the tissue. Gene expression in this  
 265 tissue shows high levels of decorin compared to  
 266 biglycan [6]. The complex arrangement of fibers  
 267 observed in costal cartilage and the role of deco-  
 268 rin and biglycan in these structures has not been  
 269 explored. We investigated the presence and distri-  
 270 bution of the different isoforms of decorin and  
 271 biglycan. This was achieved by immunohisto-  
 272 chemistry of costal cartilage from teenage  
 273 patients with pectus carinatum and an age-  
 274 matched control using antibodies to the different  
 275 isoforms of decorin and biglycan [19, 22]. Our  
 276 results (Fig. 7.5) show the presence of mature  
 277 form of decorin and pro-and mature forms of big-  
 278 glycan in the interterritorial matrix in patient and

control samples. Prodecorin was localized only  
 to the cells [19].

No apparent differences were observed  
 between an age-matched control and patient sam-  
 ples; however, proforms of decorin and biglycan  
 are maintained evolutionarily, suggesting they  
 play an important, undetermined, functional role.

Overall immunohistochemistry shows intense  
 perilacunae staining for collagen type II, mature  
 biglycan, and mature decorin. This is indicative of  
 orchestration of the ECM production occurring  
 soon after proteins are secreted from the cell.  
 Biglycan likely initiates collagen fibril organiza-  
 tion that is further assembled by decorin to form  
 the large nanostraw-like structures characteristic  
 of costal cartilage. Many other proteins will play  
 a crucial role in the final network [19, 27]. Decorin  
 and biglycan sequester TGFβ, controlling avail-  
 ability of this growth factor to chondrocytes. This  
 needs to be proven in the environment of costal  
 cartilage as it assumes the presence of this growth  
 factor within the matrix, and thus a means of  
 transport to arrive there. The components of deco-  
 rin and biglycan, (leucine rich repeats, absence or  
 presence of propeptide, and variable O-and

**Fig. 7.4** A schematic showing salient features of biglycan and decorin

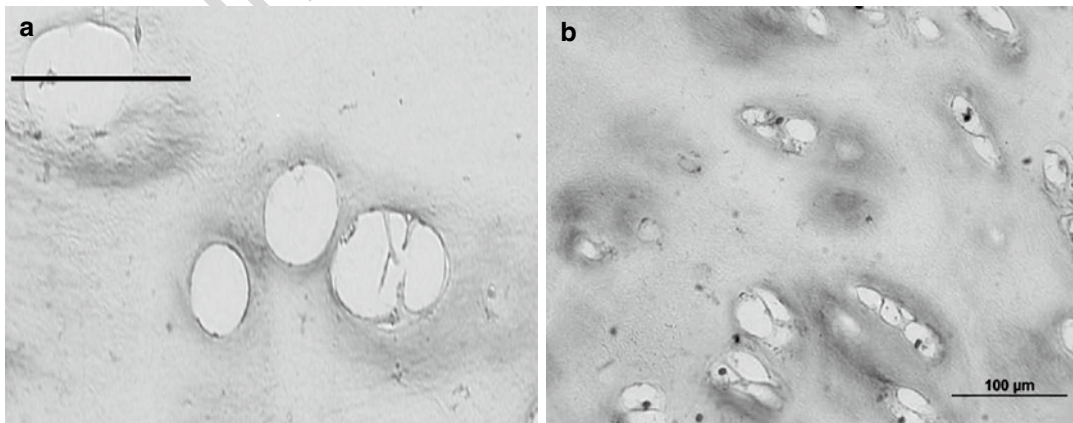
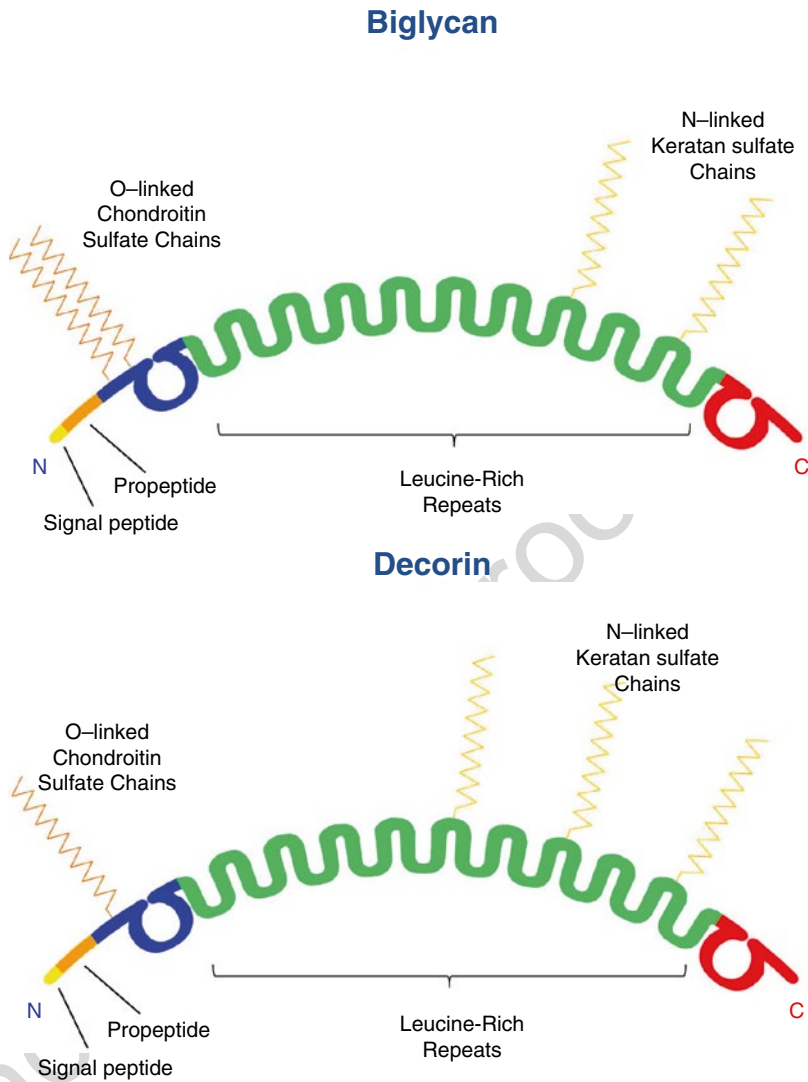


**Fig. 7.5** Detection of biglycan (LF-112, Fisher et al. 1996) (Bar 50 µm) and decorin (LF-136, Fisher et al. 1996) (Bar 100 µm). Both show dark staining around

lacunae, however decorin appears to be slightly more intense and more widely distributed



304 N-linked glycosylated side chains), allow for mul- 349  
305 tiple interactions with collagen fibrils and may be 350  
306 an important factor in cartilage stability in rela- 351  
307 tion to formation of chest wall deformities. 352  
308 Careful analysis of the composition of GAG side- 353  
309 chains may be warranted as the sugar content of 354  
310 such chains has been suggested to play a role in 355  
311 binding of collagen fibers and pathology [28]. 356

---

## 312 Glycosylation

313 Increasing attention is being given to the glyco- 357  
314 sylated side chains of proteins, particularly with 358  
315 relevance to disease [29]. Differences in side 359  
316 chains of decorin and biglycan have been 360  
317 described from different cartilage sites, includ- 361  
318 ing non-glycosylated decorin and biglycan in 362  
319 nucleus pulposus of intervertebral discs [30]. 363  
320 Decorin has a single O- and three N-linked gly- 364  
321 cosylation sites. Biglycan has two O-linked and 365  
322 two N-linked sites. O-linked sites are typically 366  
323 covalently bound by chondroitin/dermatan sul- 367  
324 phate (Fig. 7.4). Dermatan sulphate is linked to 368  
325 these molecules in skin where defects of glyco- 369  
326 sylation have been described in Ehlers Danlos 370  
327 syndrome underlying collagen fibrillogenesis 371  
328 [28]. In cartilage chondroitin sulphate is cova- 372  
329 lently bound in the O-position. Glycanated side 373  
330 chains show length variation, with shorted chains 374  
331 being associated with tighter collagen fiber con- 375  
332 figuration [31]. More recent work [32] has shown 376  
333 that decorin may bind to one collagen fibril by its 377  
334 core protein and to another by its side chain. 378  
335 Additionally, they demonstrate that closely 379  
336 related side chain molecules (chondroitin-4-sul- 380  
337 phate and chondroitin-6-sulphate) have very dif- 381  
338 ferent effects affecting fusion and layout of 382  
339 collagen fibers. This exemplifies the importance 383  
340 of recognizing subtle variations in these mole- 384  
341 cules and their biological consequences in addi- 385  
342 tion to enzyme systems that are responsible for 386  
343 synthesis and assembly of these molecules. 387  
344 Sulphate anion transporter abnormalities have 388  
345 been described in chondrodysplasias [29]. 389  
346 Interestingly, a recent report [33] describes a 390  
347 mutation in the GAL3ST4 gene in a single 391  
348 Chinese family showing dominant inheritance of 392

pectus excavatum. GAL3ST4 is a member of the 349  
350 sulfotransferase family that catalyzes the C-3 350  
351 sulfation of galactoses in O-linked glycopro- 351  
352 teins. Sulfation of proteoglycans is crucial for 352  
353 normal development of bone and cartilage [34], 353  
354 and defects in genes encoding catalytic machin- 354  
355 ery responsible for sulphate biosynthesis have 355  
356 been reported [35, 36]. The inheritance of chest 356  
357 wall deformity is extremely complex [19, 37, 357  
358 38], however the importance of the role of 358  
359 enzymes responsible for glycosylation cannot be 359  
360 overlooked and this report [33] may be corrobo- 360  
361 rated with other genes on these pathways. 361

---

## Scanning Electron Microscopy

362  
363 Suggestions that atypical collagen fibers may be 363  
364 implicated in chest wall deformities led us to 364  
365 investigate ultrastructural aspects of costal carti- 365  
366 lage. Scanning electron microscopy (SEM) was 366  
367 undertaken on a transverse section of costal carti- 367  
368 lage to investigate distribution of collagen 368  
369 fibers in this tissue. Figures 7.6a, b are represen- 369  
370 tative SEM images of a transverse cross-section 370  
371 of costal cartilage. Figure 7.6a shows a fracture 371  
372 in the cartilage exposing collagen fibers of 372  
373 approximately 600 nm diameter. Fibers come 373  
374 together to form an extremely large complex of 374  
375 many  $\mu\text{m}$  (arrowed) that run parallel to the 375  
376 length of the cartilage. Figure 7.6b is a higher 376  
377 magnification of the boxed area and shows that 377  
378 each fiber forms a nanostraw of approximately 378  
379 650 nm external diameter and 250 nm internal 379  
380 lumen diameter. Images of longitudinal sections 380  
381 show a well-defined organization with bundles 381  
382 of collagen fibers of approximately 20  $\mu\text{m}$  diam- 382  
383 eter and cellular lacunae, arrowed in Fig. 7.6c. 383

384 We measured the diameters from 150 clearly 384  
385 defined fibers from SEM images and found that 385  
386 most (51.1%) were in the range from 1 to 386  
387 100  $\mu\text{m}$ . The smallest ( $<0.1 \mu\text{m}$ ) would most- 387  
388 likely represent collagen fibrils, the midsize 388  
389 ( $\sim 1 \mu\text{m}$ ) would represent the microtubes and the 389  
390 largest ( $\sim 100 \mu\text{m}$ ) would be large fascicle-like 390  
391 structures [6]. 391

392 This work shows unique ultra-structural 392  
393 properties of costal cartilage. The presence of 393

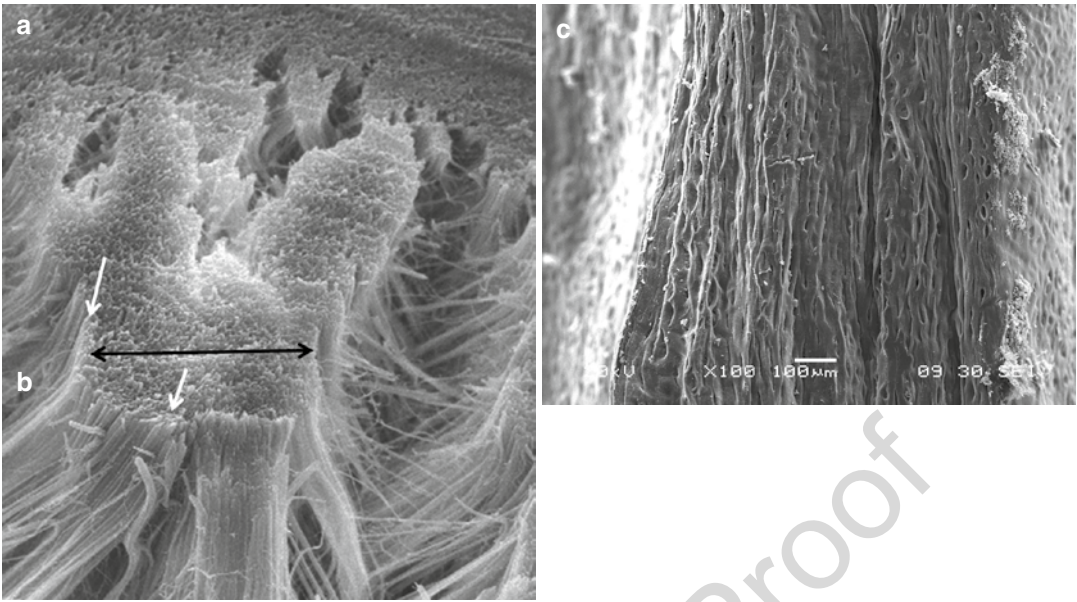


**Fig. 7.6** SEM images of normal costal cartilage. (a) Transverse section ( $\times 2500$ ) showing large numbers of dense fibrils running longitudinally (arrowed). (b) Magnification ( $\times 10,000$ ) of the boxed area in a and shows the presence of collagen nanostraws (arrowed). Each

straw is approximately 650 nm in diameter, with a lumen diameter of approximately 250 nm. (c) Longitudinal section ( $\times 500$ ) showing large bundles of collagen fibers, formed from multiple collagen nanostraws, of approximately  $20\ \mu\text{m}$  diameter (white arrow)

394 straw-like structures shows that a large degree of  
 395 complex extracellular matrix formation occurs.  
 396 Form and function are inextricably linked in biol-  
 397 ogy and the role of these structures remains to  
 398 be verified. Bundles of fluid filled straws would  
 399 certainly add strength while allowing flexibility  
 400 during movement. Indeed, movement may be a  
 401 driving force for fluid transport within costal car-  
 402 tilage, allowing some degree of nutrient and gas  
 403 exchange for internally located cells. Assuming  
 404 that the strength of costal cartilage is related to  
 405 the sum of individual nanostraws, or conversely  
 406 that weakness may be reflected in a more deform-  
 407 able nanostraw, we set out to determine mechani-  
 408 cal properties of individual nanostraws. Young's  
 409 modulus is a means to measure the elastic prop-  
 410 erties of materials that are stretched and com-  
 411 pressed and can be described as

412 Stress ( $\text{N}/\text{m}^2$ ) expressed as force (F)/area ( $\text{m}^2$ )

413 Strain (m/m) expressed as elongation or com-  
 414 pression of object (dL)/length of object (L).

415 Young's modulus = stress/strain =  $(F/A)/(\Delta L/L)$

416 Stress and strain are resisted by collagen fibers  
 417 and changes in the properties of collagen fibers  
 418 would influence Young's modulus. Many  
 419 pathological processes change tissue elasticity  
 420 and is the basis of palpitation as a diagnostic tool.  
 421 Some interesting values for Young's modulus are  
 422 given in Table 7.1, where low values are derived  
 423 from compliant materials, and high values from  
 424 resilient material.

425 Cartilage values in Table 7.1 are for articular  
 426 cartilage, however, reported values depend very  
 427 much on biological sample preparation and mea-  
 428 surement technique [39]. Our rationale for atomic

**Table 7.1** Example of a range of Young's moduli from compliant rubber to hardened steel [6]

| Material        | Approximate Young's modulus ( $10^9\ \text{N}/\text{m}^2$ ; GPa) |                      |
|-----------------|--|----------------------|
| Bone            | 9  | t1.3<br>t1.4<br>t1.5 |
| Cartilage       | 2.4  | t1.6                 |
| Tendon          | 5.5  | t1.7                 |
| Rubber          | 0.01–0.1   | t1.8                 |
| Pine wood       | 9  | t1.9                 |
| Stainless steel | 180  | t1.10                |

429 force microscopy was that individual nanostraws  
430 would have characteristic Young's modulus of  
431 elasticity, and that these may be reduced in sam-  
432 ples from patients with chest wall deformities  
433 due to abnormalities in the assembly of  
434 nanostraws. Costal cartilage from patients with  
435 chest wall deformities have often been described  
436 as weak, particularly in those who do not do well  
437 in surgery.

### 438 Atomic Force Microscopy

439 The atomic force microscope (AFM) is a very  
440 high resolution scanning probe microscope that  
441 has found applications from the biological to the  
442 material sciences and has several advantages over  
443 transmission and scanning electron microscopy,  
444 including the absence of electron-induced speci-  
445 men damage, ambient operation, preservation of  
446 biological morphology, and the ability to be uti-  
447 lized on live or fixed tissues. Analysis of biologi-  
448 cal samples frequently necessitates their fixation  
449 and protein cross-linking by chemical fixation,  
450 although fixation itself can cause tissue distor-  
451 tion. The AFM probes the surface topography of  
452 a sample to a very high resolution irrespective of  
453 whether the tissue is live or fixed. Probing of live  
454 tissues opens the possibility of investigating bio-  
455 mechanical measurements, for example, Young's  
456 modulus of elasticity [40–42]. Because AFM  
457 probing can be undertaken when the sample is  
458 submerged, it is possible to maintain live samples  
459 under physiological conditions.

460 It was proposed that the straw-like structures  
461 observed in costal cartilage act as a means of  
462 nutrient and gas transport; additionally they pro-  
463 vide biomechanical support [6]. This is analo-  
464 gous to the pressure induced fluid flow in the  
465 canaliculi-lacunae network described in bone  
466 [43]. Here stress induced microcirculation in can-  
467 aliculi of approximately 200  $\mu\text{m}$  in diameter was  
468 investigated to show that flow can nourish 4–5  
469 layers of concentric osteocytes and also suggest  
470 that stress induced flow may be important in bone  
471 remodeling where lack of flow may have patho-  
472 logical consequences, e.g., osteoporosis. Further  
473 characterization of collagen nanostraws is war-

474 ranted if such a model is to be applied to fluid  
475 flow in costal cartilage.

476 In order to further characterize collagen  
477 nanostraws, brief homogenization and enzymatic  
478 digestion of cartilage with trypsin and hyaluroni-  
479 dase was used to isolate individual samples [44].  
480 Individual nanostraws were examined for D-zone  
481 spacing and Young's modulus of elasticity.  
482 D-Zone bands are characteristic of collagen  
483 fibers, reflect the underlying regular arrangement  
484 of fibrils, and are estimated to be approximately  
485 67 nm in hydrated and 64 nm in dehydrated sam-  
486 ples [45]. The D-Zone patterns were measured  
487 from an SEM image compared to a digested and  
488 homogenized AFM image in air (Figs. 7.7a, b,  
489 respectively) and found mean D-Zone values of  
490 63 nm and 65 nm from 10 zones each. These  
491 results are consistent with shorter D-Zones in  
492 dehydrated collagen forms suggesting that the  
493 underlying arrangement of fibers in costal carti-  
494 lage derived from a patient with pectus carinatum  
495 is comparable to normal values under these  
496 conditions.

497 To determine Young's modulus of elasticity,  
498 individual isolated nanostraws were attached  
499 onto poly-L-lysine cover glass. Force measure-  
500 ments were performed using frequency modula-  
501 tion force spectroscopy [46], and the resulting  
502 force data was modeled using the Derjagin,  
503 Muller, Toropov (DMT) model [47–49] via an in-  
504 house data analysis program written in  
505 MATLAB<sup>®</sup> (version 2009, Mathworks).  
506 Figure 7.8 shows typical force measurement on a  
507 nanostraw for digested, homogenized and fixed  
508 specimen in air. Utilizing the DMT model the  
509 modulus of elasticity from six separate measure-  
510 ments is found to be  $2.06 \pm 0.35$  GPa.

511 Collagen nanostraws are structures signifi-  
512 cantly larger than individual collagen fibers and  
513 may be cross-linked by many structural proteins.  
514 Force measurements published in the literature,  
515 conducted for dehydrated collagen fibrils  
516 obtained from the common sea cucumber and  
517 analyzed at ambient conditions, resulted in val-  
518 ues ranging between 1 and 11.5 GPa [50–52].  
519 These values are high compared to reported  
520 hydrated, unfixed samples, where values of  
521 2–5 MPa are reported [53]. These values strongly

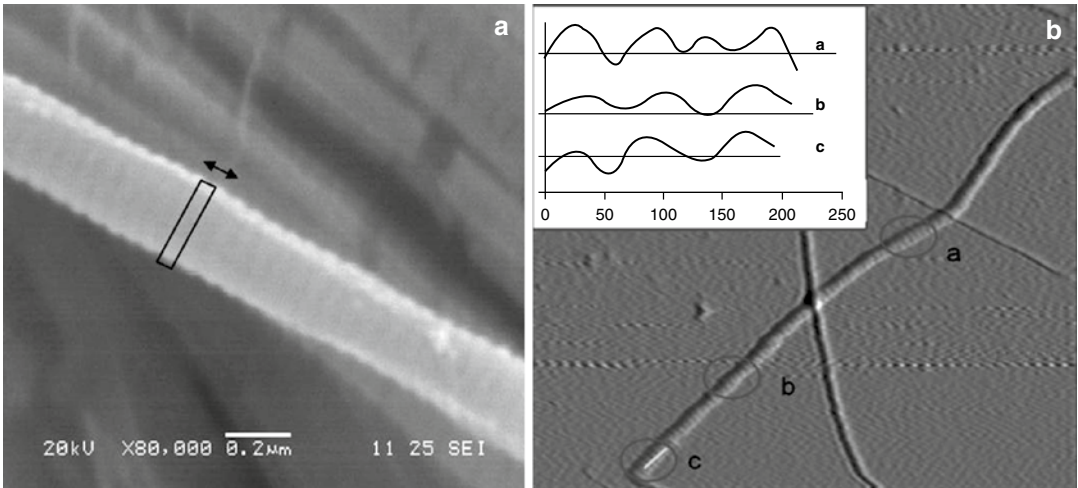


**Fig. 7.7** SEM (a) and AFM (b) of characteristic D-zones of collagen fibers. A single D-zone is blocked and arrowed in a. The insert in b shows variation in D-zones over a single fiber [44]

522 depend upon ionic concentration, hydrogen  
 523 bonding, and hydration forces, all of which can  
 524 influence interactions of tropocollagen molecules  
 525 and, therefore, the elastic modulus. High values  
 526 observed in Fig. 7.8 from costal cartilage  
 527 (23 MPa) are derived from fixed samples, and  
 528 due to cross-linking of proteins, create a more  
 529 ridged structure and thus a higher Young's  
 530 modulus.

531 Overall, these results show the unusual tubular  
 532 network of costal cartilage that is hypothesized  
 533 to act as a means of fluid and gas transport.  
 534 To study nano-fluidic transport, such structures  
 535 necessitate the accurate measurements of their  
 536 dimensions. Interestingly, previous reports suggest  
 537 that in rabbit tibia these structures correspond  
 538 to the known biomechanical properties of the  
 539 tissue, and would act as a dampening system  
 540 during compression by resisting lateral fluid  
 541 flow in the tissue and directing it against the  
 542 compressive force [54]. Our study demonstrates  
 543 that the protocols adopted for these measurements  
 544 have significant influence on size measurement.  
 545 Clearly, costal cartilage has large fiber  
 546 dimensions with complex structures that are  
 547 formed through finely tuned fibrillogenesis that  
 548 ultimately reflect the biology of this understudied  
 549 tissue type. The complex inheritance of chest  
 550 wall deformities suggests that these processes  
 551 are under the control of many genes.

### Analysis of Candidate Genes

552

553 Aggrecan is an integral part of cartilage and mutations  
 554 in the *ACAN* gene are associated with skeletal  
 555 dysplasias [55, 56]. Patients with pectus  
 556 excavatum commonly exhibit scoliosis, and *ACAN*  
 557 has been investigated as a candidate gene in familial  
 558 idiopathic scoliosis [57, 58]. The CS1 domain  
 559 of the *ACAN* gene exhibits length polymorphisms  
 560 due to a variable number of tandem repeats  
 561 (VNTR), 19 amino acids in length. Each repeat  
 562 acts as an attachment site for chondroitin sulphate  
 563 [59]. The number of *ACAN* VNTRs determines  
 564 the number of GAG side-chains. The presence on  
 565 aggrecan of a large number of highly charged  
 566 chondroitin sulphate chains generates an osmotic  
 567 swelling pressure and is important in maintaining  
 568 structural integrity of the tissue. Smaller repeat  
 569 sequences may result in mechanical shearing and  
 570 tearing [60], and are associated with rheumatoid  
 571 arthritis and spinal disc degeneration [56, 61]. It  
 572 was hypothesized that abnormalities of costal  
 573 cartilage in patients with pectus excavatum may be  
 574 due to variation in number of repeat sequences  
 575 outside of the normal reported range of 26–28 [59,  
 576 62] that would result in a concomitant change in  
 577 chondroitin sulphate anchorage sites and compromised  
 578 structural characteristics.

579 For this investigations were performed on the  
 580 size and frequency distribution of *ACAN* VNTRs

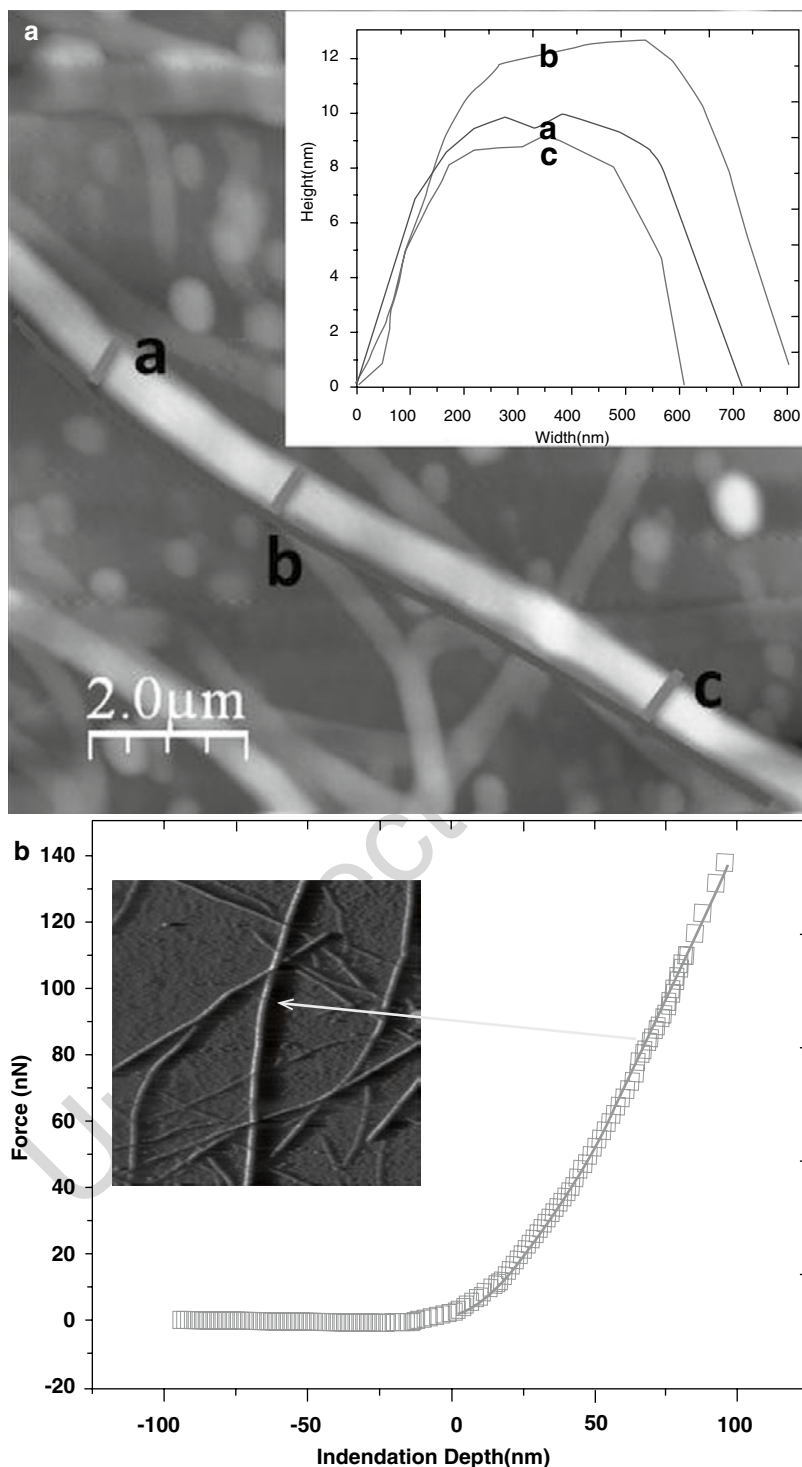


**Fig. 7.8** (a) Representative topography of costal cartilage digested and homogenized. Contrast covers height variation of 390 nm. *Insets* in the figures show height distribution of nanostraws at various locations. (b) Force versus indentation depth data on a nanostraw for homogenized

digested fixed sample in PBS buffer. Analysis based on the DMT model gives the modulus of elasticity of  $E = 23 \pm 3$  MPa in PBS buffer. Experimental data is shown by symbols, while the curve-fit of data to the DMT model is shown by *solid lines* [44]

581 in patients with pectus excavatum and correlated  
 582 overall allele sizes (genotype) to Haller index  
 583 (Fig. 7.9) [63]. This was achieved by isolating  
 584 DNA from venous blood of patients or by isolation  
 585 from chondrocytes derived from patient costal  
 586 cartilage and amplifying VNTR regions by  
 587 polymerase chain reaction (PCR) [59, 62].

588 Genotyping identified 15 alleles ranging from  
 589 19 to 34 repeats, with alleles 25–28 accounting  
 590 for 94% and 84.7% respectively in patients and  
 591 controls. Allele distribution differed between  
 592 patient and control groups ( $\chi^2=48.58$ ,  $p<.009$ )  
 593 such that patients had 0.43 fold fewer 25 repeats  
 594 ( $\chi^2=7.41$ ,  $p<.025$ ) and 1.5 fold more 27 repeat  
 595 alleles ( $\chi^2=145.32$ ,  $p<.001$ ) compared to controls.  
 596 Overall, however, we observe an allele frequency  
 597 of 0.120, 0.866, and 0.014 in patients for  
 598 <26, 26–28, and >28 alleles respectively, consistent  
 599 with the normal observed range [59, 62].  
 600 There is no apparent bias of allele genotype with  
 601 increased Haller index, therefore a specific  
 602 combination of VNTRs does not predispose to  
 603 increased severity in pectus excavatum.

604 Patients showed phenotypic variation, and  
 605 subgroups were identified where a genetic component  
 606 may be influential. Females (16% of  
 607 patients), showed a significant increase in severity  
 608 compared to males ( $t(250)=2.36$ ,  $p<.019$ ;  
 609 Mean+SD: 5.7+2.1 vs. 4.8+2.2), and tended to  
 610 have a decreased number of VNTRs, consistent

611 with a hypothesis of reduced attachment sites for  
 612 chondroitin sulphate and weakened cartilage.

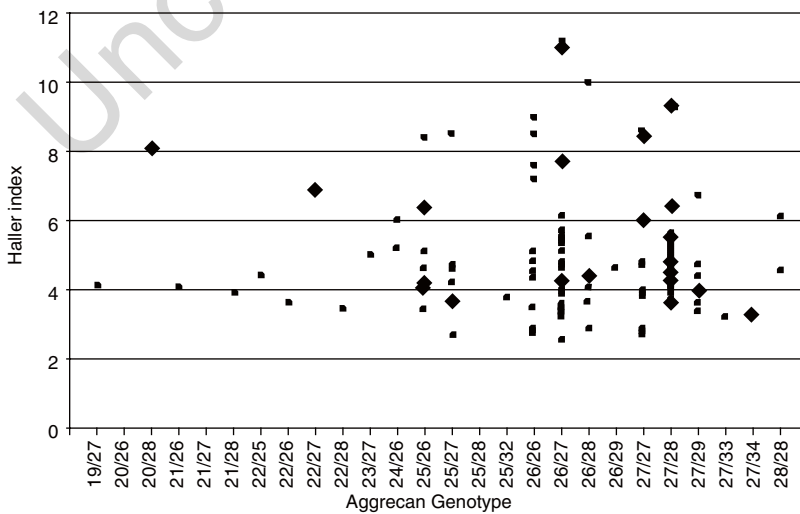
613 Marfan phenotype patients (10.4% of  
 614 patients), exhibited phenotypic findings consistent  
 615 with Marfan appearance such as long limbs,  
 616 arachnodactyly and high-arched palate without  
 617 absolute diagnostic criteria for Marfan syndrome  
 618 [64]. There was no apparent correlation in the  
 619 number of VNTRs compared to the non-Marfan  
 620 patients, suggesting that VNTRs do not have a  
 621 differential role in this subgroup.

622 Repeat surgeries are the smallest subgroup (3.2%  
 623 of patients) and showed no correlation between  
 624 Haller index and surgical outcome, suggesting initial  
 625 presentation is not an indicator of outcome.

626 Furthermore variation in a functional VNTR  
 627 were investigated and identified, a useful marker  
 628 for first-pass analysis. Investigation of SNPs will  
 629 allow a more refined description in the inheritance  
 630 of this, and other candidate genes, in the  
 631 role of inherited chest wall deformities.

632 **Analysis of Gene Expression in Costal**  
 633 **Cartilage**

634 Cartilage formation is a complex process with  
 635 many interacting components. To determine gene  
 636 expression in costal cartilage investigations were  
 637 performed on twelve candidate genes based upon



638 **Fig. 7.9** Correlation of aggrecan genotype (VNTR repeats/allele) with Haller index in male (squares) and female (diamonds) patients [63]

638 structural and functional importance in cartilage  
 639 formation. Table 7.2 lists each gene and chromo-  
 640 somal location. Chest wall deformities show a  
 641 sex bias, being more prevalent in males compared  
 642 to females (4:1) [37, 38], suggesting that genes  
 643 located on chromosome X may be of importance.  
 644 Males have a single X chromosome (XY) and  
 645 therefore defects in genes on this chromosome  
 646 cannot be compensated for by genes at a second  
 647 allele as in females (XX). Four genes were identi-  
 648 fied on chromosome X with relevance to carti-  
 649 lage formation (Table 7.2).

650 *Aggrecan*: A large aggregating proteoglycan that  
 651 serves to anchor highly negatively charged  
 652 keratin and chondroitin sulphate molecules  
 653 ultimately responsible for generating osmotic  
 654 pressure within cartilage.

655 *Biglycan*: *BGN*, a SLRP on the X-chromosome  
 656 that encodes for the protein involved in assem-  
 657 bly of collagen fibrils within the extracellular  
 658 matrix of cartilage. It is closely related to  
 659 decorin, possibly through gene duplication,  
 660 and carries two glycosaminoglycan side  
 661 chains. It strongly binds the growth factor  
 662 TGF- $\beta$ , controlling bioavailability.

663 *Tissue inhibitor of metalloproteinase-1*: *TIMP1*  
 664 is located on the X chromosome and plays a  
 665 role in the maintenance and turnover of the  
 666 extracellular matrix within cartilage. It func-  
 667 tions as an inhibitor of matrix metalloprotein-  
 668 ases (MMPs), specifically MMP-8 and  
 669 MMP-13, which are both collagenases.

*Voltage-gated calcium channel- $\alpha 1F$* : *CACNA1F* 670  
 671 is a gene that encodes for a voltage-gated cal-  
 672 cium channel and is found on the X chromo-  
 673 some. It functions to control the amount of  
 674 calcium that enters the cell upon membrane  
 675 polarization and may be linked to bioelectric  
 676 components of cartilage.

677 *Nyctalopin*: The *NYX* gene was investigated  
 678 because of its location on the X chromosome  
 679 and its function as a SLRP. It is associated  
 680 more with eye function, and defects in the  
 681 gene result in a number of eye related anoma-  
 682 lies including night blindness

683 *Collagen  $\alpha$ -1 chain*: *COL1A1* encodes for Type I  
 684  $\alpha$  collagen fiber found in most connective tis-  
 685 sues. Although not expressed highly in articu-  
 686 lar cartilage, it acts as a marker of cartilage  
 687 differentiation.

688 *Collagen type II  $\alpha$ -1*: *COL2A1* encodes for col-  
 689 lagen Type II- $\alpha$  fibers found in cartilage where  
 690 mutations in this gene have been associated  
 691 with chondrodysplasias. It is highly expressed  
 692 in articular cartilage and is essential for carti-  
 693 lage to resist compressive forces.

694 *Decorin*: *DCN* is a SLRP that plays a role in  
 695 matrix assembly. It has an important role in  
 696 binding collagen fibrils and strongly influ-  
 697 ences fiber size and shape. It has a single gly-  
 698 cosaminoglycan side chain. It binds to  
 699 COL1A1, COL2A1 and the growth factor  
 700 TGF- $\beta$ , controlling bioavailability.

701 *Fibrillin 1*: *FBN1* encodes a large matrix proteo-  
 702 glycan that serves as a structural component in

**Table 7.2** Candidate genes investigated in this study [6]

| Gene                          | Name                                       | Chromosome location |
|-------------------------------|--|---------------------|
| <i>ACTB</i>                   | $\beta$ -Actin                             | 7p22                |
| <i>ACAN</i>                   | Aggrecan                                   | 15q26.1             |
| <i>BGN</i>                    | Biglycan                                   | Xq28                |
| <i>CACNA1F</i>                | Voltage-gated calcium channel- $\alpha 1F$ | Xp11.23             |
| <i>COL1A1</i>                 | Collagen $\alpha$ -1 chain                 | 17q21.33            |
| <i>COL2A1</i>                 | Collagen type II $\alpha$ -1               | 12q13.11            |
| <i>DCN</i>                    | Decorin                                    | 12q21.33            |
| <i>FBN1</i>                   | Fibrillin 1                                | 15q21.1             |
| <i>NYX</i>                    | Nyctalopin                                 | Xp11.4              |
| <i>SOX9</i>                   | SRY (Sex determining region Y)-box 9       | 17q24.3             |
| <i>TGF<math>\beta</math>1</i> | Transforming Growth Factor- $\beta$ 1      | 19q13.2             |
| <i>TIMP1</i>                  | Tissue inhibitor of metalloproteinase 1    | Xp11.23             |

703 force bearing microfibrils and binds to TGF-  
704 beta. Mutations in this gene are associated  
705 with Marfan syndrome where chest wall  
706 defects are common. One of these mutations  
707 creates an N-glycosylation site that disrupts  
708 multimeric assembly [28].

709 *Sex determining region SRY box-9: SOX9* is a  
710 homeobox class of DNA binding proteins. It is  
711 a potent activator of *COL2A1* and may also  
712 regulate the expression of other genes involved  
713 in cartilage formation by acting as a transcrip-  
714 tion factor for these genes.

715 *Transforming Growth Factor-β1: TGFβ1* is a  
716 multifunctional protein that controls prolifera-  
717 tion and differentiation in many cell types. It  
718 regulates many other growth factors, and stim-  
719 ulates chondrocyte cell growth through the  
720 MAPK3 signaling pathway.

721 *β-Actin: ACTB*, was used throughout as a reference  
722 housekeeping gene and from which relative lev-  
723 els of gene expression were calculated.

724 For this, costal cartilages were immediately  
725 placed into a solution of RNAlater after surgery  
726 to preserve the integrity of expressed genes. RNA  
727 was extracted as described previously [6]. RNA  
728 was reverse transcribed to produce cDNA and  
729 amplified by RT-PCR on a BioRad CFX96 real  
730 time system (Fig. 7.10). Gene expression was  
731 measured by incorporation of SYBR green into

732 amplified products. All primers were designed  
733 specifically for gene amplification (Qiagen CA,  
734 USA). Relative fold differences in gene expres-  
735 sion were calculated as  $2^{-\text{(CtGOI - CtHKG)}}$ , where  
736 CtGOI is the Ct value of the gene of interest com-  
737 pared to the CtHKG, which is the Ct value for the  
738 house keeping gene [65].

739 Costal cartilage from individuals with chest  
740 wall deformities is described as abnormally grown  
741 and weak. Typically, surgical repair takes place  
742 during teenage years to early 20s. Phenotypically,  
743 there is considerable variation of the clinical con-  
744 dition of PC, reflecting the complex nature and  
745 inheritance observed in these families. Variation  
746 in gene expression between samples is, therefore,  
747 expected; however, it is unknown whether the  
748 expression of matrix genes will be affected by  
749 surgical procedures. We compared gene expres-  
750 sion of 4 patients with pectus carinatum to an age-  
751 matched-control. *COL2A1*, *DCN*, *ACAN*, and  
752 *TIMP1* are all highly expressed compared to  
753 *ACTB*, however, when normalized to control  
754 (=100%) significant reductions in expression are  
755 observed with sample variation (Table 7.3).

756 Compared to control, PC1 showed significant  
757 reduction in expression of *DCN* ( $p < 0.001$ ) and  
758 *TIMP1* ( $p < 0.001$ ). PC3 showed significantly  
759 lower expression of *COL2A1* ( $p < 0.001$ ) and like  
760 PC4, both showed decreased expression of *ACAN*  
761 ( $p < 0.03$  and  $p < 0.024$ , respectively). PC4 also

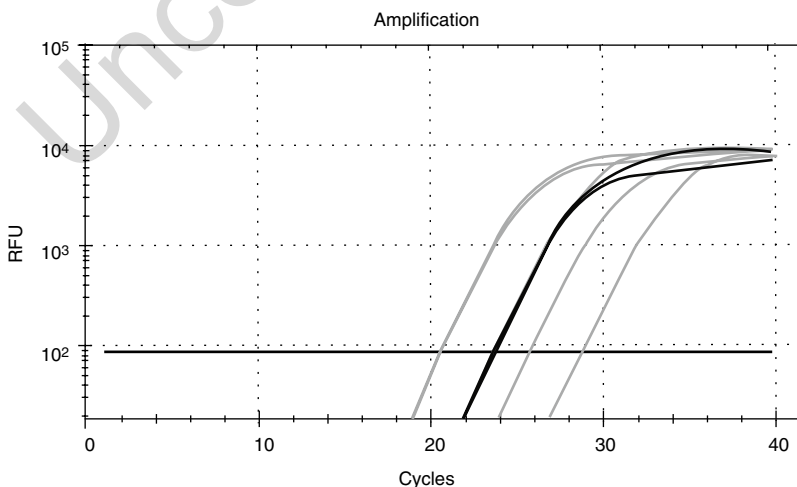


**Fig. 7.10** Gene expression curves showing left to right, expression of *DCN*, *TIMP-1* (overlapping *actin*) *ACTB*, *BGN*, and *TGFβ*. High expression is displayed as a curve farthest to the left and lower expression moving to the right



762 showed significantly higher expression of *TIMP1*  
 763 ( $p < 0.001$ ) and decreased expression of *BGN*  
 764 ( $p < 0.04$ ). PC2 showed significant reduction in  
 765 expression of *COL2A1* ( $p < 0.01$ ), *DCN*  
 766 ( $p < 0.0002$ ), *TIMP1* ( $p < 0.001$ ), *BGN* ( $p < 0.03$ )  
 767 and *FBN1* ( $p < 0.01$ ). This sample, like all PC  
 768 samples, was immediately processed from the  
 769 operating room, although results suggest possible  
 770 degradation of this sample.

771 Many patients with chest wall deformities are  
 772 considered Marfanoid-like [64] without fulfilling  
 773 all criteria for diagnosis of Marfan syndrome,  
 774 including mutations of the fibrillin-1 gene. The  
 775 expression of this gene was not significantly dif-  
 776 ferent between control and patients, with the  
 777 exception of PC2 ( $p < 0.01$ ). Expression of the  
 778 X-linked genes *NYX* and *CACNA1F* was not  
 779 detected in any samples. Overall, deregulation of  
 780 *TIMP1* expression was evident in 3/4 PC sam-  
 781 ples, and expression of *DCN* was significantly  
 782 lower in 2/4, suggestive of roles for fibrillo-  
 783 genesis and matrix turnover.

t3.1 **Table 7.3** Percent fold difference in gene expression of  
 t3.2 four patients with pectus carinatum compared to  $\beta$ -actin  
 t3.3 and normalized to an age-matched control

|                                      | PC1 | PC2 | PC3 | PC4  |
|--------------------------------------|-----|-----|-----|------|
| t3.4 <i>COL2A1</i>                   | 100 | *63 | *35 | 89   |
| t3.5 <i>ACAN</i>                     | 122 | 93  | *42 | *205 |
| t3.6 <i>DCN</i>                      | *25 | *25 | 92  | 117  |
| t3.7 <i>TIMP1</i>                    | *21 | *29 | 107 | *174 |
| t3.8 <i>ACTB</i>                     | 100 | 100 | 100 | 100  |
| t3.9 <i>BGN</i>                      | 43  | *24 | 60  | *22  |
| t3.10 <i>COL1A1</i>                  | 125 | 100 | 92  | 100  |
| t3.11 <i>FBN1</i>                    | NA  | *39 | 107 | 65   |
| t3.12 <i>SOX9</i>                    | 91  | 61  | 46  | 191  |
| t3.13 <i>TGF-<math>\beta</math>1</i> | 83  | 72  | 50  | 22   |

t3.15 Significant differences in expression between control and  
 t3.16 patients are marked with \* [6]

784 The differentiation status of cartilage can be  
 785 equated to the ratio of *COL2A1*, present in dif-  
 786 ferentiated cartilage, to *COL1A1*, present at  
 787 higher levels in more undifferentiated cartilage.  
 788 We compared ratios of gene expression from our  
 789 samples to published data.

790 Ratios of the differentiation markers  
 791 *COL2A1:ACAN* and *COL2A1:COL1A1* are low in  
 792 PC patients and control (Table 7.4) compared to  
 793 rabbit articular cartilage (1090 and 1790, respec-  
 794 tively) but both are highly comparable to the  
 795 nucleus pulposus region of lumbar discs (23 and  
 796 930 respectively), [66]. The ratios of  
 797 *ACAN:COL1A1* fall between those reported for  
 798 fully differentiated rat chondrosarcoma cells (78.4)  
 799 and dedifferentiated chondrocytes cultured from  
 800 costal cartilage (4.6) [67]. A high expression ratio  
 801 of *COL2A1:COL1A1* (294.6) in human articular  
 802 cartilage has been reported [65], but here results are  
 803 referenced to *GAPDH* rather than *ACTB*. Overall,  
 804 these results suggest costal cartilage is at an inter-  
 805 mediate stage of differentiation and likely repre-  
 806 sents the different functional requirements of this  
 807 tissue compared to articular cartilage. The differen-  
 808 tiation similarities between lumbar discs and costal  
 809 cartilage are of interest. The high incidence of sco-  
 810 liosis in patients with chest wall deformities indi-  
 811 cates that defects of cartilage of a specific  
 812 differentiation status may be very important. Small  
 813 differences exist however between patients and  
 814 between patients and control (Table 7.4), suggest-  
 815 ing that gene ratios measured here are not major  
 816 contributors to chest wall abnormalities in these  
 817 samples. Interestingly, *DCN* is expressed at high  
 818 levels compared to *BGN*. As well as binding growth  
 819 factors, both SLRPs have a role in fibrillogenesis  
 820 and were hypothesized to play a role in the etiology  
 821 of chest wall deformities. The high *DCN/BGN*  
 822 ratio strongly suggests the importance of decorin

**Table 7.4** Gene expression ratios in costal cartilage from pectus carinatum and age-matched control

|         | <i>COL2A1/ACAN</i> | <i>COL2A1/COL1A1</i> | <i>ACAN/COL1A1</i> | <i>DCN/BGN</i> |
|---------|--------------------|----------------------|--------------------|----------------|
| PC1     | 35                 | 878                  | 25                 | 8              |
| PC2     | 29                 | 701                  | 24                 | 13             |
| PC3     | 36                 | 427                  | 12                 | 19             |
| PC4     | 19                 | 990                  | 53                 | 69             |
| Control | 43                 | 1117                 | 26                 | 13             |

823 expression in costal cartilage morphology. Decorin  
824 is present at high levels during tendon (fibro-  
825 cartilage) development and persists until thick  
826 fibers are formed [17], thus parallels with costal  
827 cartilage (hyaline cartilage) are apparent.

### 828 Conclusions

829 Biological properties of human costal cartilage  
830 are a much understudied field. In this  
831 chapter preliminary data that investigates these  
832 properties were described. Sample character-  
833 ization is of utmost importance and future  
834 studies should attempt to utilize samples from  
835 different but identified ribs, and the site of  
836 control samples should be verified for com-  
837 parative purposes. Acquisitions of healthy age  
838 match controls are not easy because the age  
839 of patients tend to be teens to twenties. It has  
840 been suggested that rib abnormalities may be  
841 secondary to events of the thorax, with costal  
842 cartilage responding to micro-environmental  
843 factors, changing their biological characteris-  
844 tics as a result. The 'chicken and egg' paradox  
845 needs to be resolved, and identification of bio-  
846 logical causes identified. This is particularly  
847 relevant to patients who do not do well in sur-  
848 gery, where a biological basis may underlie  
849 their prognosis and outcomes.

850 **Acknowledgments** Thanks go to the Center for  
851 Bioelectrics, Old Dominion University for their support,  
852 particularly the Director, Dr. Richard Heller. Additional  
853 thanks go to Anthony Asmar for his dedication in the labo-  
854 ratory and help in this manuscript. I would also like to thank  
855 surgeons who provided samples, specifically, Drs Kelly Jr,  
856 Nuss, Franz, and Obermeyer of the Children's Hospital of  
857 the King's Daughters, Norfolk, VA, USA, and Dr Annie  
858 Fecteau of the Hospital for Sick Children, Toronto, Canada.  
859 Thanks also to collaborators at Old Dominion University,  
860 Norfolk VA, especially Dennis Darby, Ali Beskok, and  
861 Hani Elsayed Ali. Particular thanks to Dr Marian Young  
862 and Dr Larry Fisher of the NIDCR, NIH, Bethesda, MD,  
863 USA for their help, encouragement, and antibodies to iso-  
864 forms of decorin and biglycan.

### 865 References

866 1. Schumacher BL, Su JL, Lindley KM, Kuettner KE,  
867 Cole AA. Horizontally oriented clusters of multiple  
868 chondrons in the superficial zone of ankle, but not  
869 knee articular cartilage. *Anat Rec.* 2002;266:241–8.

2. Jadin KD, Wong BL, Bae WC, Li KW, Williamson 870  
AK, Schumacher BL, Price JH, Sah RL. Depth- 871  
varying density and organization of chondrocytes in 872  
immature and mature bovine articular cartilage 873  
assessed by 3d imaging and analysis. *J Histochem* 874  
*Cytochem.* 2005;53:1109–19. 875

3. Clark JM, Rudd E. Cell patterns in the surface of rab- 876  
bit articular cartilage revealed by the backscatter 877  
mode of scanning electron microscopy. *J Orthop Res.* 878  
1991;9:275–83. 879

4. Rolauﬀs B, Williams JM, Grodinsky AJ, Kuettner 880  
KE, Cole AA. Distinct horizontal patterns in the spa- 881  
tial organization of superficial zone chondrocytes of 882  
human joints. *J Struct Biol.* 2008;162:335–44. 883

5. Chi SS, Rattner JB, Matyas JR. Communication 884  
between paired chondrocytes in the superficial zone 885  
of articular cartilage. *J Anat.* 2004;205:363–70. 886

6. Stacey MW, Grubb J, Asmar A, Pryor J, Elsayed-Ali 887  
H, Cao W, Beskok A, Dutta D, Darby DA, Fecteau A, 888  
Werner A, Kelly Jr RE. Decorin expression, straw- 889  
like structure, and differentiation of human costal car- 890  
tilage. *Connect Tissue Res.* 2012;53(5):415–21. 891

7. Feng J, Hu T, Liu W, Zhang S, Tang Y, Chen R, Jiang 892  
X, Wei F. The biomechanical, morphologic, and his- 893  
tochemical properties of the costal cartilages in chil- 894  
dren with pectus excavatum. *J Pediatr Surg.* 2001;36: 895  
1770–6. 896

8. Fokin AA, Nury M, Steuerwald M, Ahrens William A, 897  
Allen KE. Anatomical, Histologic, and genetic char- 898  
acteristics of congenital chest wall deformities. *Semin* 899  
*Thorac Cardiovasc Surg.* 2009;21(1):44–57. 900

9. Rupprecht H, Hümmer HP, Stöß H, Waldherr 901  
T. Pathogenesis of the chest wall deformities – elec- 902  
tron microscope studies and analysis of trace elements 903  
in the cartilage of the ribs. *Eur J Pediatr Surg.* 904  
1987;42(4):228–9. 905

10. Forman JL, del Pozo de Dios E, Dalmases CA, Kent 906  
RW. The contribution of the perichondrium to the 907  
structural mechanical behavior of the costal-cartilage. 908  
*J Biomech Eng.* 2010;132:094501 doi:10.1115/ 909  
1.4001976. 910

11. Sun DD, Guo XE, Likhitpanichkul M, Lai WM, Mow 911  
VC. The influence of the fixed negative charges on 912  
mechanical and electrical behaviors of articular carti- 913  
lage under unconfined compression. *J Biomech Eng.* 914  
2004;126:6–16. 915

12. Das RHJ, van Osch GJVM, Kreukniet M, Oostra J, 916  
Weinans H, Jahr H. Effects of individual control of pH 917  
and hypoxia in chondrocyte culture. *J Orthop Res.* 918  
2010;28:537–45. 919

13. Duval E, Leclercq S, Elissalde JM, Demoor M, Galera 920  
P, Boumediene K. Hypoxia-inducible factor 1 $\alpha$  inhib- 921  
its the fibroblast-like markers type I and type III col- 922  
lagen during hypoxia-induced chondrocyte 923  
redifferentiation. *Arthritis Rheum.* 2009;60:3038–48. 924

14. Cheng C, Uchiyama Y, Hiyama A, Gajghate S, 925  
Shapiro IM, Risbud MV. PI3K/AKT regulates aggre- 926  
can gene expression by modulating Sox9 expression 927  
and activity in nucleus pulposus cells of the interver- 928  
tebral disc. *J Cell Physiol.* 2009;221:668–76. 929

- 930 15. Ameye L, Young MF. Mice deficient in small  
931 leucine-rich proteoglycans: novel in vivo models  
932 for osteoporosis, osteoarthritis, Ehlers-Danlos syn-  
933 drome, muscular dystrophy, and corneal diseases.  
934 *Glycobiology*. 2002;12:107R-16.
- 935 16. Embree MC, Kilts TM, Ono M, Inkson CA, Syed-  
936 Picard F, Karsdal MA, Oldberg A, Bi Y, Young  
937 MF. Biglycan and fibromodulin have essential roles in  
938 regulating chondrogenesis and extra cellular matrix  
939 turnover in temporomandibular joint osteoarthritis.  
940 *Am J Pathol*. 2010;176:812-26.
- 941 17. Kalamajski S, Oldberg A. The role of small leucine-  
942 rich proteoglycans in collagen fibrillogenesis. *Matrix*  
943 *Biol*. 2010;29:248-53.
- 944 18. Melrose J, Fuller ES, Roughley PJ, Smith MM, Kerr  
945 B, Hughes CE, Caterson B, Little CB. Fragmentation  
946 of decorin, biglycan, lumican and keratocan is ele-  
947 vated in degenerate human meniscus, knee and hip  
948 articular cartilages compared with age-matched mac-  
949 roscopically normal and control tissues. *Arthritis Res*  
950 *Ther*. 2008;10:R79.
- 951 19. Asmar A, Werner A, Kelly Jr RE, Fecteau A, Stacey  
952 M. Presence and localization of pro and mature forms  
953 of decorin and biglycan in human costal cartilage  
954 derived from chest wall deformities. *Aust*  
955 *J Musculoskel Disord*. 2015;2(1):1012.
- 956 20. Heegaard AM, Corsi A, Danielsen CC, Nielsen KL,  
957 Jorgensen HL, Riminucci M, Young MF, Bianco  
958 P. Biglycan deficiency causes spontaneous aortic dis-  
959 section and rupture in mice. *Circulation*. 2007;115:  
960 2731-8.
- 961 21. Bianco P, Fisher LW, Young MF, Termine JD, Robey  
962 PG. Expression and localization of the two small pro-  
963 teoglycans biglycan and decorin in developing human  
964 skeletal and non-skeletal tissues. *J Histochem*  
965 *Cytochem*. 1990;38:1549-63.
- 966 22. Fisher LW, Stubbs JT, Young MF. Antisera and cDNA  
967 probes to human and certain animal model bone  
968 matrix noncollagenous proteins. *Acta Orthopediatr*  
969 *Scand*. 1995;66:61-5.
- 970 23. von Marschall Z, Fisher LW. Decorin is processed  
971 by three isoforms of bone morphogenetic protein-1  
972 (BMP1). *Biochem Biophys Res Commun*. 2010;391:  
973 1374-8.
- 974 24. Krishnan P, Hocking AM, Scholtz JM, Pace CN,  
975 Holik KK, McQuillan DJ. Distinct secondary struc-  
976 tures of the leucine-rich repeat proteoglycans decorin  
977 and biglycan. Glycosylation-dependent conforma-  
978 tional stability. *J Biol Chem*. 1999;274(16):10945-50.
- 979 25. Roughley PJ, White RJ, Mort JS. Presence of pro-  
980 forms of decorin and biglycan in human articular car-  
981 tilage. *Biochem J*. 1996;318:779-94.
- 982 26. Götz W, Barnert S, Bertagnoli R, Miosge N, Kresse H,  
983 Herken R. Immunohistochemical localization of the  
984 small proteoglycans decorin and biglycan in human  
985 intervertebral discs. *Cell Tissue Res*. 1997;289:185-90.
- 986 27. Roughley PJ. Articular cartilage and changes in  
987 arthritis; noncollagenous proteins and proteoglycans  
988 in the extracellular matrix of cartilage. *Arthritis Res*.  
989 2001;3:342-7.
28. Freeze HH, Schachter H. Genetic disorders of glyco- 990  
sylation. Chapter 42. In: Varki A, Cummings RD, 991  
Esko JD, et al., editors. *Essentials of glycobiology*. 992  
2nd ed. Cold Spring Harbor: Cold Spring Harbor 993  
Laboratory Press; 2009. 994
29. Rhodes J, Campbell BJ, Yu LG. Glycosylation and 995  
disease. *Encyclopedia of Life Sciences (eLS)*. 996  
Chichester: Wiley; 2010. doi:10.1002/9780470015902. 997  
a0002151.pub2. 998
30. Johnstone B, Markopoulos M, Neame P, Caterson 999  
B. Identification and characterization of gly- 1000  
canated and non-glycanated forms of biglycan and 1001  
decorin in human intervertebral discs. *Biochem* 1002  
*J*. 1993;292:661-6. 1003
31. Scott JE. Morphometry of cupromeronic blue-stained 1004  
proteoglycan molecules in animal corneas, versus that 1005  
of purified proteoglycans stained in vitro implies that 1006  
tertiary structures contribute to corneal ultrastructure. 1007  
*J Anat*. 1992;180:155-64. 1008
32. Raspanti M, Viola M, Forlino A, Tenni R, Gruppi C, 1009  
Tira ME. Glycosaminoglycans show a specific peri- 1010  
odic interaction with type I collagen fibrils. *J Struct* 1011  
*Biol*. 2008;164:134-9. 1012
33. Wu S, Sun X, Zhu W, Huang Y, Mou L, Liu M, Li X, 1013  
Li F, Li X, Zhang Y, Wang Z, Li W, Li Z, Tang A, Gui 1014  
Y, Wang R, Li W, Cai Z, Wang D. Evidence for 1015  
GAL3ST4 mutation as the potential cause of pectus 1016  
excavatum. *Cell Res*. 2012;22:1712-5. doi:10.1038/ 1017  
cr.2012.149. 1018
34. Honke K, Taniguchi N. Sulfotransferases and sulfated 1019  
oligosaccharides. *Med Res Rev*. 2002;22:637-54. 1020
35. Kurima K, Warman ML, Krishnan S, Domowicz M, 1021  
Krueger Jr RC, Deyrup A, Schwartz NB. A member of 1022  
a family of sulfate-activating enzymes causes murine 1023  
brachymorphism. *Proc Natl Acad Sci U S A*. 1024  
1998;95:8681-5. 1025
36. Superti-Furga A, Hästbacka J, Wilcox WR, Cohn DH, 1026  
van der Harten HJ, Rossi A, Blau N, Rimoin DL, 1027  
Steinmann B, Lander ES, Gitzelmann 1028  
R. Achondrogenesis type IB is caused by mutations in 1029  
the dystrophic dysplasia sulphate transporter gene. 1030  
*Nat Genet*. 1996;12:100-2. 1031
37. Creswick H, Stacey M, Kelly R, Burke B, Gustin T, 1032  
Mitchell K, Nuss D, Harvey H, Croitoru D, Goretzky 1033  
M, Vasser E, Fox P, Goldblatt S, Tabangin M, Proud 1034  
V. Family studies on the inheritance of pectus excava- 1035  
tum. *J Pediatr Surg*. 2006;41:1699-703. 1036
38. Horth L, Stacey MW, Benjamin T, Segna K, Proud VK, 1037  
Nuss D, Kelly RE. Genetic analysis of inheritance of 1038  
pectus excavatum. *J Pediatr Genet*. 2012;1(3):161-73. 1039
39. McKee CT, Last JA, Russell P, Murphy 1040  
CJ. Indentation versus tensile measurements of 1041  
Young's modulus for soft biological tissues. *Tissue* 1042  
*Eng B*. 2011;17(3):155-64. 1043
40. Stolz M, Raiteri R, Daniels AU, VanLandingham 1044  
MR, Baschong W, Aebi U. Dynamic elastic modu- 1045  
lus of porcine articular cartilage determined at two 1046  
different levels of tissue organization by indentation 1047  
type atomic force microscopy. *Biophys J*. 2004;86: 1048  
3269-83. 1049

- 1050 41. Cai X, You P, Cai J, Yang X, Chen Q, Huang F. ART-  
1051 induced biophysical and biochemical alterations of  
1052 jurkat cell membrane. *Micron*. 2011;42:17–28.
- 1053 42. Tripathy S, Berger EJ. Quasi-linear viscoelastic prop-  
1054 erties of costal cartilage using atomic force micros-  
1055 copy. *Comput Methods Biomech Biomed Engin*.  
1056 2012;15:475–86.
- 1057 43. Kufahl RH, Saha S. A theoretical model for stress-  
1058 generated fluid flow in the canaliculi-lacunae network  
1059 in bone tissue. *J Biomech*. 1990;23:171–80.
- 1060 44. Stacey M, Dutta D, Cao W, Asmar A, El-Sayed Ali H,  
1061 Kelly Jr R, Beskok A. Atomic force microscopy char-  
1062 acterization of collagen ‘nanostraws’ in human costal  
1063 cartilage. *Micron*. 2013;44:483–7.
- 1064 45. Orgel JPRO, San Antonio JD, Antipova O. Molecular  
1065 and structural mapping of collagen fibril interactions.  
1066 *Connect Tissue Res*. 2011;52:2–17.
- 1067 46. Sader JE, Jarvis SP. Accurate formulas for interaction  
1068 force and energy in frequency modulation force spec-  
1069 troscopy. *Appl Phys Lett*. 2004;84(10):1801–3.
- 1070 47. Derjaguin BV, Muller VM, Toporov YP. Effect of con-  
1071 tact deformations on the adhesion of particles.  
1072 *J Colloid Interface Sci*. 1975;53(2):314–26.
- 1073 48. Maugis D. Adhesion of spheres: the JKR-DMT transi-  
1074 tion using a dugdale model. *J Colloid Interface Sci*.  
1075 1991;150:243–69.
- 1076 49. Grierson DS, Flater EE, Carpick RW. Accounting for  
1077 the JKR-DMT transition in adhesion and friction  
1078 measurements with atomic force microscopy.  
1079 *J Adhesion Sci Technol*. 2005;19(3–5):291–311.
- 1080 50. Heim AJ, Mathews WG, Koob TJ. Determination of  
1081 the elastic modulus of native collagen fibrils via radial  
1082 indentation. *Appl Phys Lett*. 2006;89:181902–4.
- 1083 51. Heim AJ, Koob TJ, Mathews WG. Low strain nano-  
1084 mechanics of collagen fibrils. *Biomacromolecules*.  
1085 2007;8:3298–301.
- 1086 52. Wenger MP, Bozec EL, Horton MA, Mesquida  
1087 P. Mechanical properties of collagen fibrils. *Biophys*  
1088 *J*. 2007;93:1255–63.
- 1089 53. Grant CA, Brockwell DJ, Radford SE, Thomson  
1090 NH. Tuning the elastic modulus of hydrated collagen  
1091 fibrils. *Biophys J*. 2009;97:2985–92.
- 1092 54. ap Gwynn I, Wade S, Ito K, Richards RG. Novel  
1093 aspects to the structure of rabbit articular cartilage.  
1094 *Eur Cell Mater*. 2002;2:18–29.
- 1095 55. Gleghorn L, Ramesar R, Beighton P, Wallis G. A  
1096 mutation in the variable repeat region of the aggrecan  
1097 gene (AGC1) causes a form of spondyloepiphyseal  
1098 dysplasia associated with severe, premature osteoar-  
1099 thritis. *Am J Hum Genet*. 2005;77(3):484–90.
- 1100 56. de Souza TB, Mentz EF, Brenol CV, Xavier RM,  
1101 Brenol JC, Chies JA, Simon D. Association between  
1102 the aggrecan gene and rheumatoid arthritis.  
1103 *J Rheumatol*. 2008;35(12):2325–8.
- 1104 57. Marosy B, Justice CM, Nzegwu N, Kumar G, Wilson  
1105 AF, Miller NH. Lack of association between the  
1106 aggrecan gene and familial idiopathic scoliosis.  
1107 *Spine*. 2006;31(13):1420–5.
- 1108 58. Merola A, Mathur S, HaHer T, Espat NJ. Polymorphism  
1109 of the aggrecan gene as a marker for adolescent idio-  
1110 pathic scoliosis. *Scoliosis Research Society*. Quebec  
1111 City; 2003.
- 1112 59. Roughley P, Martens D, Rantakokko J, Alini M,  
1113 Mwale F, Antoniou J. The involvement of the aggrecan  
1114 polymorphism in degeneration of human interverte-  
1115 bral disc and articular cartilage. *Eur Cells Mater*.  
1116 2006;11:1–7.
- 1117 60. Kawaguchi Y, Osada R, Kanamori M, Ishihara H,  
1118 Ohmori K, Matsui H, Kimura T. Association between  
1119 aggrecan gene polymorphism and lumbar disc degener-  
1120 eration. *Spine*. 1999;24:2456–60.
- 1121 61. Solovieva S, Noponen N, Männikkö M, Leino-Arjas  
1122 P, Luoma K, Raininko R, Ala-Kokko L, Riihimäki  
1123 H. Association between the aggrecan gene variable  
1124 number of tandem repeats polymorphism and inter-  
1125 vertebral disc degeneration. *Spine (Phila Pa 1976)*.  
1126 2007;32(16):1700–5.
- 1127 62. Doege KJ, Coulter SN, Meek LM, Maslen K, Wood  
1128 JG. A human-specific polymorphism in the coding  
1129 region of the aggrecan gene. Variable number of tan-  
1130 dem repeats produce a range of core protein sizes in  
1131 the general population. *J Biol Chem*. 1997;272:  
1132 13974–9.
- 1133 63. Stacey M, Neumann S, Dooley A, Segna K, Kelly R,  
1134 Nuss D, Kuhn A, Goretsky M, Fecteau A, Pastor A,  
1135 Proud V. Variable number of tandem repeat polymor-  
1136 phisms (VNTRs) in the ACAN gene associated with  
1137 pectus excavatum. *Clin Genet*. 2010;78:502–4.
- 1138 64. Redlinger Jr RE, Rushing GD, Moskowitz AD, Kelly  
1139 Jr RE, Nuss D, Kuhn A, Obermeyer RJ, Goretsky  
1140 MJ. Minimally invasive repair of pectus excavatum in  
1141 patients with Marfan Syndrome and Marfanoid fea-  
1142 tures. *J Pediatr Surg*. 2010;45(1):193–9.
- 1143 65. Martin I, Jakob M, Schafer D, Dick W, Spagnoli G,  
1144 Heberer M. Quantitative analysis of gene expression  
1145 in human articular cartilage from normal and osteoar-  
1146 thritic joints. *Osteoarthritis Cartilage*. 2001;9:112–8.
- 1147 66. Clouet J, Grimandi G, Pot-Vaucel M, Masson M,  
1148 Fellah HB, Guigand L, Cheral Y, Bord E, Rannou F,  
1149 Weiss P, Guicheux J, Vinatier C. Identification of phe-  
1150 notypic discriminating markers for intervertebral disc  
1151 cells and articular chondrocytes. *Rheumatology*.  
1152 2009;48(11):1447–50.
- 1153 67. McAlinden A, Havlioglu N, Liang L, Davies SR,  
1154 Sandell LJ. Alternative splicing of type II procollagen  
1155 exon 2 is regulated by the combination of a weak 5’  
1156 splice site and an adjacent intronic stem-loop Cis ele-  
1157 ment. *J Biol Chem*. 2005;280:32700–11.

# Author Queries

Chapter No.: 7      0002824519

| Queries | Details Required  | Author's Response |
|---------|---|-------------------|
| AU1     | Please confirm if identified heading levels are okay.   |                   |
| AU2     | Please provide artwork for part figures “d–h” of Fig. 7.2.                                    |                   |
| AU3     | Please provide caption for part figures “a and b” of Figs. 7.4 and 7.5.                       |                   |
| AU4     | “Fisher et al. (1996)” is cited in text but not provided in the reference list. Please check. |                   |
| AU5     | Please confirm the inserted citation for Table 7.3.   |                   |
| AU6     | Kindly provide the significance of arrows for Figs. 7.2.                                      |                   |

Uncorrected Proof